AMERICAN SCIENTIFIC PUBLISHERS

Energy and Environment Focus
Vol. 2, pp. 112–120, 2013
(www.aspbs.com/efocus)

ARTICLE

Electrochemical Properties and Electrochromic Behaviors of the Sol–Gel Derived Tungsten Trioxide Thin Films

Huige Wei[1,2], Xingru Yan[1,2], Qiang Wang[3], Shijie Wu[4], Yuanbing Mao[5], Zhiping Luo[6], Haoran Chen[7], Luyi Sun[8], Suying Wei[2,*], and Zhanhu Guo[1,*]

[1]*Integrated Composites Laboratory (ICL), Dan F. Smith Department of Chemical Engineering, Lamar University, Beaumont, TX 77710, USA*
[2]*Department of Chemistry and Biochemistry, Lamar University, Beaumont, TX 77710, USA*
[3]*Environmental Functional Nanomaterials (EFN) Laboratory, College of Environmental Science and Engieering, Beijing Forestry University, Beijing 100083, China*
[4]*Agilent Technologies Inc., Chandler, AZ 85226, USA*
[5]*Department of Chemistry, University of Texas, Pan American, Edinburg, TX 78539, USA*
[6]*Department of Chemistry and Physics, Fayetteville State University, Fayetteville, NC 28301, USA*
[7]*Department of Chemistry and Biochemistry, Texas State University, San Marcos, TX 78666, USA*

ABSTRACT

Electrochemical properties and electrochromic (EC) behaviors of the tungsten oxide (WO_3) thin films on the indium tin oxide (ITO) coated glass slides have been studied. The thin films were prepared by simply annealing the drop casted tungsten ethoxide/ethanlol/water sol thin films. The effects of the annealing conditions on the thin film morphology, phase structure and the subsequent electrochemical properties and the electrochromic behaviors have been systematically studied. The morphology and crystalline structure of the WO_3 thin films were studied by atomic force microscopy (AFM), X-ray diffraction (XRD) and transmission electron microscopy (TEM). The calcination conditions had a significant impact on the EC film structure. Thin film from 2-h 100 °C annealing exhibited an amorphous structure and evenly sized crystalline WO_3 particles for the thin film with additional 2-h 200 °C annealing. Cyclic voltammetry (CV), chronocoulometry (CC) and *in situ* spectroelectrochemistry methods were employed to study the electrochemical properties and electrochromic behaviors of these thin films in a propylene carbonate (PC) solution containing 1 M $LiClO_4$. Even though it took 30 seconds for coloration and 54 seconds for bleaching process in the thin film from additional 2-h 200 °C annealing than those (16 and 27 s) of the thin film from 2-h 100 °C annealing, the thin film with additional 2-h 200 °C annealing demonstrated a better performance in terms of higher transmittance modulation (30.5% for the thin film with additional 2-h 200 °C annealing and 21.6% for thin film from 2-h 100 °C at 685 nm) and coloration efficiency (48.3 cm^2 C^{-1} for the thin film with additional 2-h 200 °C annealing and 40.2 cm^2 C^{-1} for thin film from 2-h 100 °C). The higher electrochemical activity and better cycling durability render it promising as smart windows for solar light control and energy saving applications.

KEYWORDS: Tungsten Oxide, Sol–Gel, Electrochromic Film, Smart Window.

1. INTRODUCTION

Electrochromism is defined as a reversible optical change, which occurs upon the reduction (gain of electrons) or oxidation (loss of electrons) upon the passage of an electrical current after the application of an appropriate electrode potential in the material.[1–3] Electrochromic (EC) materials can be classified into three groups: inorganic materials (transition metal oxides),[4,5] organic small molecules[6–8] and conjugated polymers.[9–16] Owing to its particular physicochemical properties, tungsten trioxide (WO_3) has received extensive attention for its applications in photoelectrocatalysis,[17–19] gas sensing,[20–23] EC devices,[4,24,25] automotive antidazzling rear veiw mirrors and smart windows for usage in cars and buildings. As an *n*-type semiconductor with a band-gap of 2.7 eV, WO_3 is mostly investigated among the many inorganic materials for many advantages including genuine color

*Authors to whom correspondence should be addressed.
Emails: suying.wei@lamar.edu, zhanhu.guo@lamar.edu
Received: 1 March 2013
Accepted: 14 April 2013

switching, good chemical stability and strong adherence to substrate.[26–30] It is generally accepted that the injection and extraction of electrons and metal cations plays a key role in giving the EC effect, which can be illustrated as Eq. (1):[3, 5, 30]

$$WO_3 + xM^+_{\text{Transparent}} + xe^- \rightarrow M_xW^{VI}_{(1-x)\text{blue}}W^{V}_xO_3 \quad (1)$$

with $M^+ = H^+$, Li^+, Na^+ or K^+, and e^- denoting electrons. The EC colors (blue and colorless) are derived from the intervalence charge-transfer optical transitions.[31]

EC coatings based on different WO_3 structures including nanowires,[32] nanorods,[33] and mesopores[34, 35] have been reported by the methods including hydrothermal process,[32, 33] sol–gel derived spin or dip coating method,[36, 37] sputtering,[38, 39] and wet chemical deposition.[40, 41] Organic ligands and emulsion based methods have also been employed to prepare tungsten oxides.[34, 42] However, high-temperature calcinations (higher than 500 °C) are needed to remove surfactants, which will result in a reduction of specific surface area and an increase in particle size.

Sol–gel method is the most popular for preparing EC WO_3 films for its cost effectiveness, ease of depositing uniform large films for window applications. More importantly, sol–gel method allows for obtaining films of improved properties by varying the sols or by manipulating the calcination conditions.[43–45] Sol–gel prepared from the reaction of hydrochloric acid with tungsten ethoxide were proved to be a suitable and facile way to prepare WO_3 films free of foreign ions, thus avoiding the impurity of sol–gel when the alkaline-soldium-tungstate and hydrochloric acid were used as the raw materials.[46] Although the structure change during the gelation process has been studied using X-ray diffraction and Raman spectroscopic,[47] the EC behaviors of the films have not been studied.

In this paper, transparent tungsten oxide thin films were obtained by a sol–gel process from a tungsten ethoxide/ethanlol/water solution (sol). The films were deposited onto indium tin oxide (ITO) coated glass slides by drop casting and calcined at two different conditions, one was at 100 °C for two hours and the other was calcined at 100 °C for two hours and 200 °C for additional two hours. The morphology and crystalline structure of the EC films were characterized using atomic force microscopy (AFM), X-ray diffraction (XRD) and transmission electron microscopy (TEM). The electrochemical properties, the electrochromic behaviors and cycling stability were also investigated using cyclic voltammetry (CV), chronocoulometry (CC) and *in-situ* spectroelectrochemical techniques in a polycarbonate (PC) electrolyte containing 1 M lithium per chlorate ($LiClO_4$). Switching characteristics of the films in terms of contrast modulation, coloration efficiency, and response time of the EC tungsten oxide films were obtained and compared.

2. EXPERIMENTAL DETAILS

2.1. Materials

Tungsten (VI) ethoxide was purchased from Alfar-Aesar. Lithium per chlorate ($LiClO_4$, >95%, Sigma Aldrich) and propylene carbonate (99%, Sigma Aldrich) were used as electrolyte. The microscope glass slides and indium tin oxide (ITO) coated glass slides were obtained from Fisher and NanoSci Inc, respectively. ITO coated glass slides were sonicated in ethanol for 10 min, and then immersed in an aqueous solution containing 1 mL 28.86 wt% ammonium hydroxide, 1 mL 30.0 wt% hydrogen peroxide (both from Fisher), and 5 mL deionized water for 10 min, and sonicated in deionized water for 10 min before usage.

2.2. Preparation of WO_3 Sol–Gel Film

The WO_3 sol–gel films were prepared according to the typical sol–gel method. Briefly, tungsten ethoxide (0.5 g) was dissolved in 125 mL ethanol, and was stirred at 75 °C for 3 h to obtain a clear solution. 0.5 mL distilled water containing 3.5×10^{-4} g HCl was added into the solution for hydrolysis while stirring vigorously at room temperature. The ethanol was gently evaporated until 15 mL sol solution remained. Scheme 1 illustrates the hydrolysis of tungsten ethoxide and condensation process taking place in the ethanol solution. Thin sol films on the ITO glass slides were prepared by drop casting technique. The films were calcined under two different processes. One was calcined at 100 °C for 2 h, with a light green transparent film obtained, denoted as W-1; the other one was treated by two successive calcinations of 100 °C for 2 h followed by 200 °C for another 2 h, and the film turned to light yellow, denoted as W-2.

2.3. Characterizations

The Fourier transform infrared (FT-IR) spectra of the films were obtained on a Bruker Inc. Vector 22 (coupled with an ATR accessory) in the range of 500 to 4000 cm^{-1} at a resolution of 4 cm^{-1}. X-ray diffraction (XRD) analysis was carried out with a Bruker AXS D8 Discover diffractometer with GADDS (General Area Detector Diffraction System) operating with a Cu-K_α radiation source filtered with a graphite monochromator ($\lambda = 1.5406$ Å). Data were collected in a range of 20 to 80°. Transmission electron

Hydrolysis:

$$W(OC_2H_5O)_6 + 6\,H_2O \longrightarrow W\text{-}(OH)_6 + 6\,C_2H_5OH$$

Condensation:

$$n\,W\text{-}(OH)_6 \longrightarrow (WO_3)_n + 3n\,H_2O$$

Scheme 1. Schematic illustration of preparation of WO_3 sol and gelation of the sol.

ARTICLE

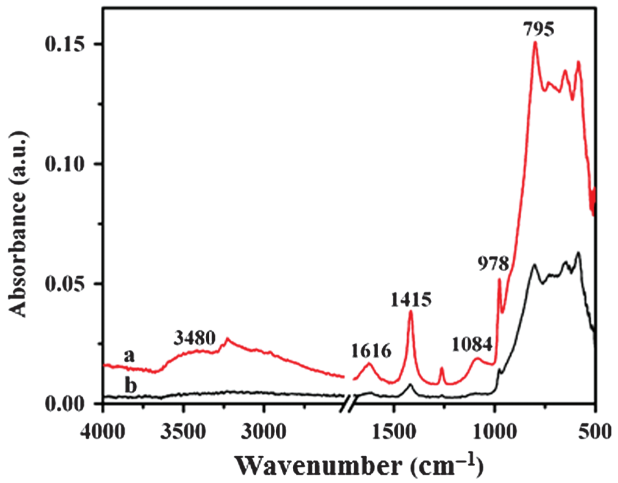

Fig. 1. IR spectra of **(a)** W-1 and **(b)** W-2.

microscopy (TEM, Philips CM-200 with a LaB6 filament and an accelerating voltage of 200 kV) was used to characterize the morphology and crystallinity of the WO_3 films. The calcined films were scratched from the glass slides and dissolved in methanol solution. The TEM samples were prepared by dropping a small amount of the WO_3 suspended methanol solution onto a carbon coated copper grid followed by drying in air at room temperature. The morphology of the thin films grown on the ITO glass slides were characterized by atomic force microscopy (AFM, Agilent 5600 AFM system with multipurpose 90 μm scanner). Imaging was done in acoustic ac mode (AAC) using a silicon tip with a force constant of 2.8 N/m and a resonance frequency of 70 kHz.

Cyclic voltammetry (CV) and chronocoulometry (CC) tests were performed in a propylene carbonate (PC) solution of 1 M $LiClO_4$ using an electrochemical working station VersaSTAT 4 potentiostat (Princeton Applied Research). CV measurements were carried out at a scanning rate of 50 mV/s between -1.0 and 1.0 V at room temperature. CC tests were conducted under a square-wave voltage of 2.0 and -2.0 V with a pulse width of 100 s. The spectroelectrochemistry measurements were performed on a Jasco V-670 spectrophotometer coupled with the potentiostat for applying electrochemical potentials. The electrochemical tests were conducted under nitrogen atmosphere.

3. RESULTS AND DISCUSSION

3.1. Structure and Morphology

3.1.1. FT-IR

Figure 1 shows the FT-IR spectra of the annealed WO_3 films of W-1 and W-2. Both films exhibit similar features of monoclinic WO_3 in the lower frequencies. The band typical of the W—O—W bonds appears in the 600–1000 cm^{-1}, with a maximum at 795 cm^{-1}.[48–50] A band at 1086 cm^{-1} and a sharp band centered around 978 cm^{-1} are assigned to W=O stretching mode,[36,51] which is common for tungsten trioxide hydrates ($WO_3 \cdot xH_2O$)[52,53] that were formed by the condensation of the sol during the annealing process. Monoclinic WO_3 is constituted by corner-sharing distorted and tilted octaedra where the W atoms are off-center, and the W—O bonds have a different length (three of them are about 1.8 Å while the other three are about 2.1 Å long).[54] When water is produced during the condensation reaction, it can occupy one axial position and the corresponding W—OH_2 bond is rather long (ca. 2.3 Å) whereas the opposite axial bond is short (ca. 1.7 Å) and is usually indicated as W=O. The W=O band can react readily with atmospheric water giving rise to W—OH bonds which can be H–bonded to water molecules forming W—OH$\cdots$$OH_2$.[51] A broad peak around 3480 cm^{-1} is assigned to the H-bonded water. Consistently, a band at 1415 cm^{-1} arising from the W—OH$\cdots$$OH_2$ [36,55] and 1616 cm^{-1} corresponding to the bending vibration of water molecules[36] are observed. W-1 and W-2 exhibit similar patterns, indicating similar molecular structure despite of different annealing conditions.

3.1.2. AFM

Figure 2 shows AFM images of (a) W-1 and (b) W-2 films. When calcined at 100 °C for 2 h, the film displays a smooth structure for W-1, Figure 2(a), and the thickness of the film was measured to be about 200 nm. As the film was subjected to further calcination at 200 °C for another 2 h, Figure 2(b), the morphology of the film undergone significant changes. Evenly sized particles began to be observed under AFM observation. Therefore, the calcination condition has a remarkable impact on the morphology of WO_3 films prepared from the sol precursor.

3.1.3. XRD and TEM

Figure 3 shows the XRD pattern of W-1 and W-2 films. As shown in Figure 3, W-1 reveals amorphous structure with no obvious diffraction peaks. Under further heating treatment, some sharp peaks corresponding to the plane (111), (002) and (200) of monoclinic WO_3 [56] appeared in W-2, Figure 3(b). The HRTEM image in Figure 4 further confirmed the crystalline structure of W-2. The lattice fringes observed in the image indicate that the film is crystallized. The lattice spacing of 0.377 and 0.382 nm corresponds to the d-spacing of (020) and (002) planes of monoclinic WO_3, respectively.[57]

3.2. Electrochemical Properties and Electrochromic Behaviors

Cyclic voltammorgrams of W-1 and W-2 were recorded at a scan rate of 50 mV/s from -1 to $+1$ V for 1000 cycles to assess the endurance of the films, which is a prime concern

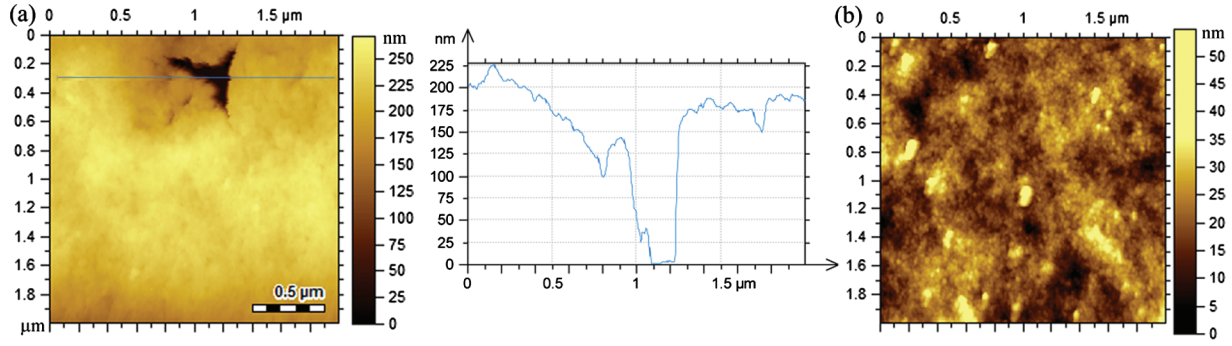

Fig. 2. AFM images of (a) W-1 and (b) W-2.

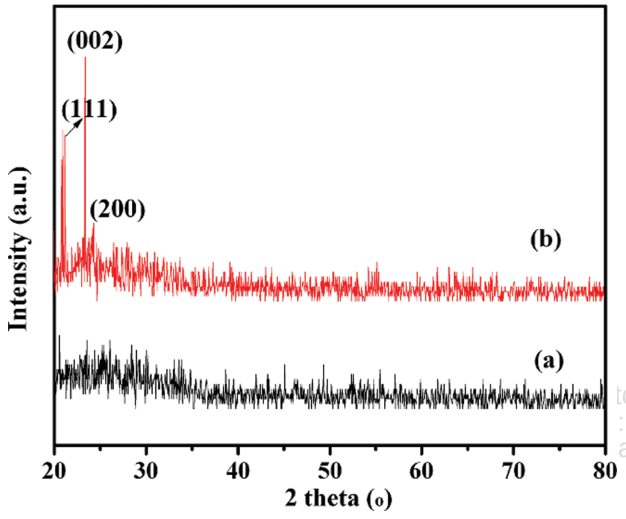

Fig. 3. XRD pattern of the annealed WO_3 sol–gel film of (a) W-1 and (b) W-2.

for WO_3 films for smart window applications.[36] Figure 5 shows the CV profile of W-1 and W-2, both of which exhibit well-defined peaks associated with the deintercalation of Li^+.[5] For W-1, the peak current density increases first and then becomes stable, indicating an activation process for the intercalation of Li^+ ions into the thin film to reach the saturation level.[58] For W-2, no activation stage occurs, and the peak current density decreases slowly in the first several cycles and then becomes reproducible from the 500th cycle until the 1000th cycle. The minor variations in the initial cycles might be attributed to some irreversible structure change in the film.[59] The absolute value of peak current gives a rough estimation of electrochemical activity of the working electrode, where a higher absolute value of peak current indicates a higher electrochemical activity, and vice versa,[60] thus it can be inferred that W-2 possesses higher electrochemical activity than W-1. The diffusion coefficient for the diffusing lithium ions can be determined from the oxidation peak current dependence on the square root of the potential sweep rate assuming simple solid state diffusion controlled phenomenon using the Randles–Servcik equation.[61]

$$i_p = 2.72 \times 10^5 n^{3/2} D^{1/2} C_o \nu^{1/2}$$

where D is the diffusion coefficient ($cm^2\ s^{-1}$), C_o is the concentration of the active ion in solution (mol cm^{-3}), ν is the sweep rate (V s^{-1}), n is the number of electrons, here

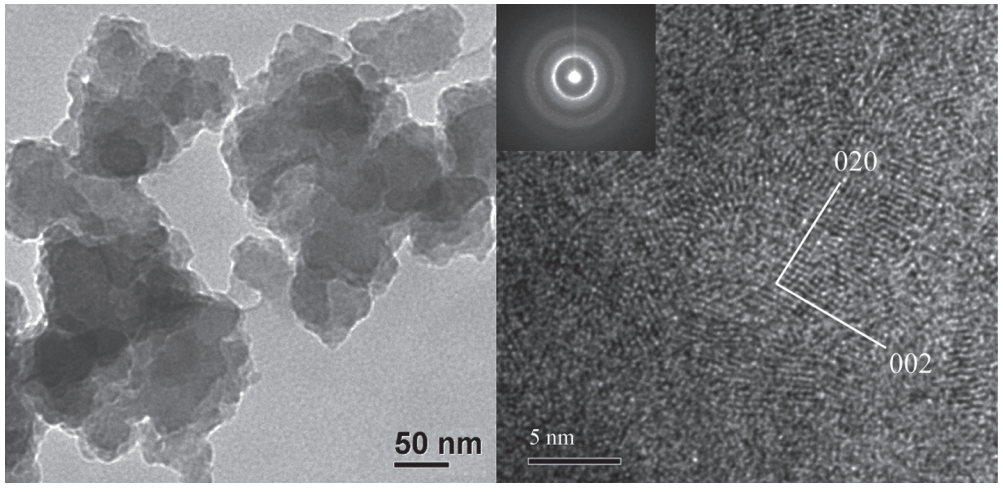

Fig. 4. TEM of the annealed WO_3 sol–gel film.

ARTICLE

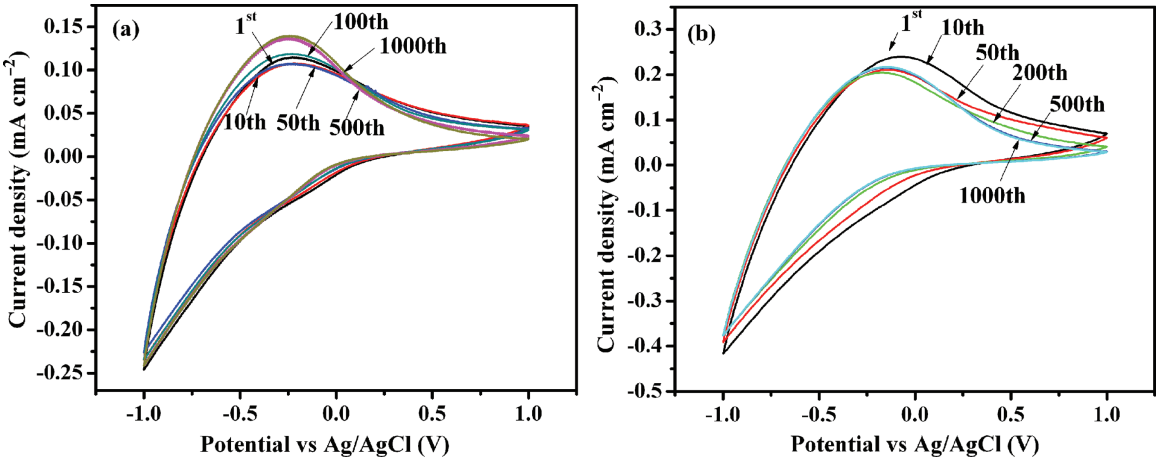

Fig. 5. Cyclic voltammograms of (a) W-1 and (b) W-2 onto ITO in propylene carbonate containing 1 M $LiClO_4$. The scan rate is 50 mV/s and the scan range is from −1 to +1 V.

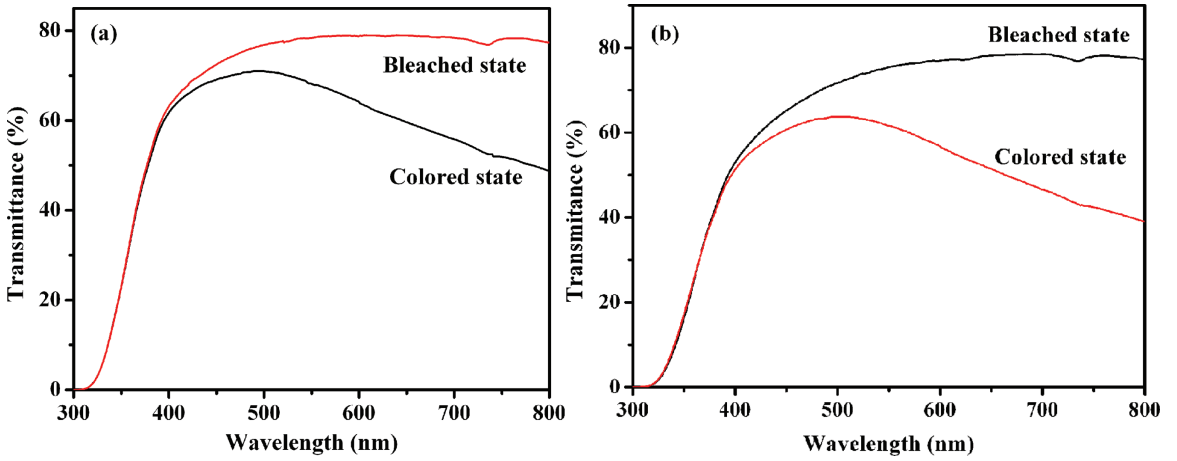

Fig. 6. UV-vis transmittance spectra of (a) W-1 and (b) W-2 at the bleached state and colored state in 1 M $LiClO_4$ propylene carbonate.

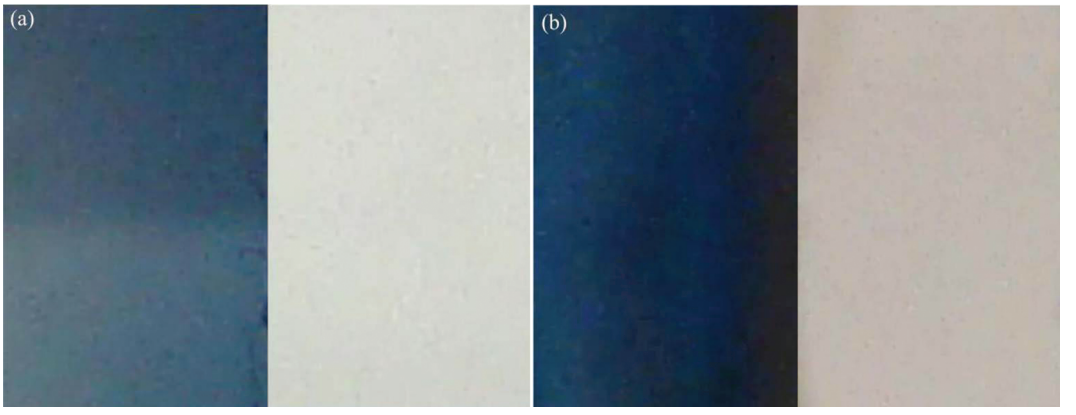

Fig. 7. Color switching of (a) W-1 and (b) W-2 films at −2 V and +2 V after 50 seconds (from left side to right side), respectively, in 1 M $LiClO_4$ propylene carbonate.

is 1, and i_p is the peak current density (A cm^{-2}). The diffusion coefficients obtained are in the order of 10^{-11} cm^2 s^{-1} (1.9×10^{-11} for W-2 and 0.5×10^{-11} cm^2 s^{-1} for W-1), which is consistent with most previous work on sol–gel based films.[62, 63]

The electrochromic behaviors and coloration-bleaching kinetics of W-1 and W-2 films were studied by chronoamperometry and the corresponding *in situ* transmittance. Figure 6 shows the UV-Vis spectra of the films at colored (generation of different visible region electronic absorption

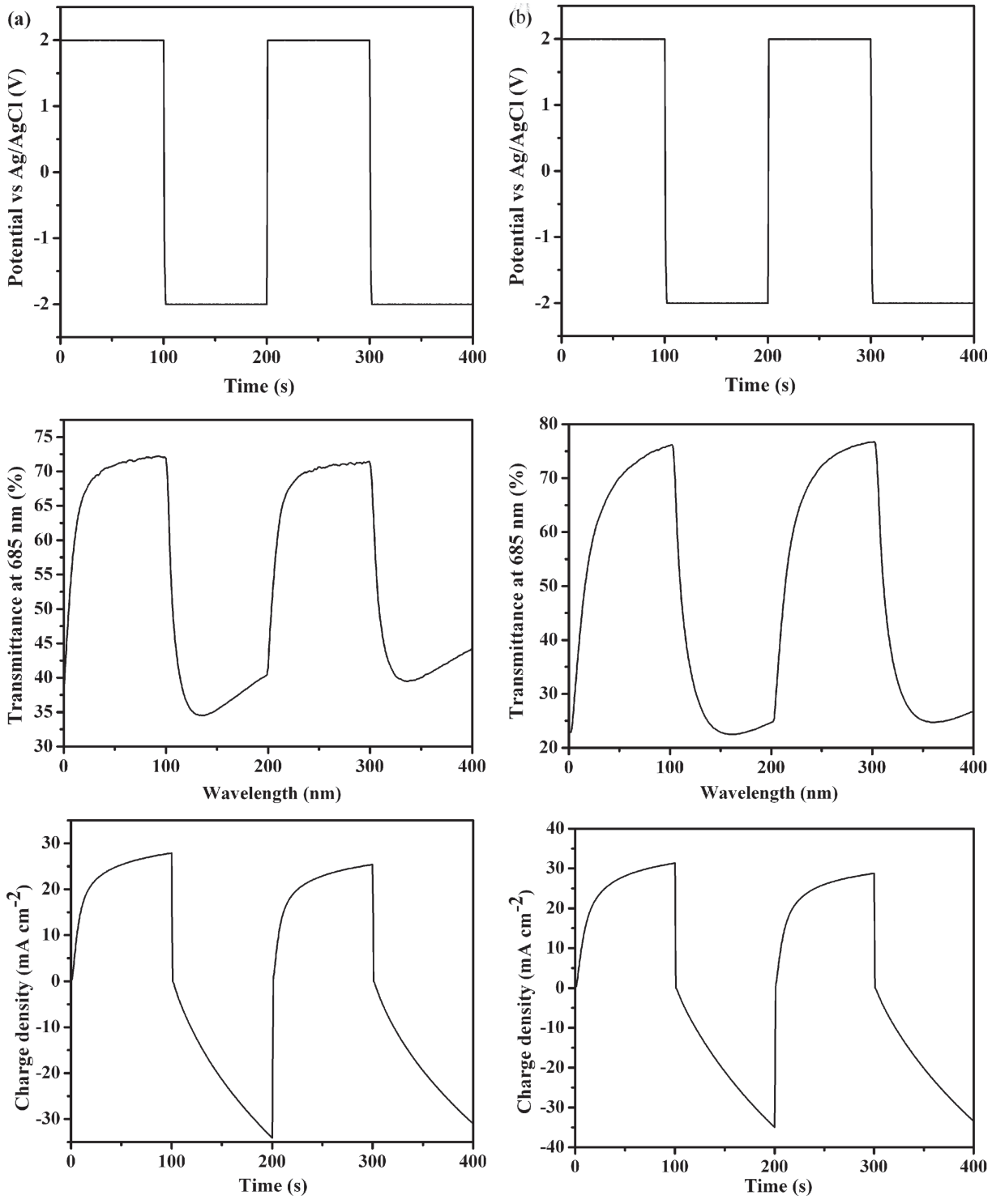

Fig. 8. Supplied step potential, chronocoulometry and the corresponding *in situ* transmittance at 685 nm of (a) W-1 and (b) W-2 films in 1 M $LiClO_4$ propylene carbonate.

ARTICLE

bands)[64] and bleached (colorless) state upon being subjected to −1 and +1 V in 1 M $LiClO_4$ propylene carbonate (PC) solution for 100 s, respectively. As shown in Figure 6, both films show a high transmittance as high as 80% at positive voltage. When applied to a negative potential, a significant absorbance in the wavelength ranging from 550 nm to near IR band caused by the Li^+ intercalation is observed.[65] W-2 displays a higher modulation range of transmittance. The percent transmittance change, %T, is 30.6% for W-2 and 21.6% for W-1 at 685 nm.

Both films turned from blue at colored state to colorless at bleached state as the potential switched from negative to positive. The color change is believed to be associated with the intercalation (deintercalation) of the Li^+ ions into (or out from) the WO_3 films:

$$WO_3 + xLi^+ + xe^-_{\text{Transparent}} \leftrightarrow \underset{\text{Blue}}{Li_xWO_3}$$

Figure 7 shows the color switching of W-1 and W-2 at −2 and +2 V (from the left side to the right side). W-2 displays more significant color change due to higher electrochemical activity from the result of CV, which is in good agreement with the higher modulation range of transmittance of W-2 in Figure 6.

Figure 8 shows the switching characteristics of the films of W-1 and W-2 using chronocoulometry and *in situ* transmittance at 685 nm. The chronocoulometry was conducted between −2.0 and +2.0 V in 1 M $LiClO_4$ polycarbonate solution in nitrogen atmosphere. For W-1, the transmittance is 72.2% at the bleached state and 34.5% at the colored state at 685 nm. For W-2, the transmittance at the bleached and colored state is 76.2% and 22.4%, respectively. Thus W-2 gives higher transmittance modulation of 53.8% while a transmittance modulation of 37.7% for W-1 can be obtained. The main difference in the transmittance at colored state may also be explained by the fact of more intercalation of the Li^+ ions into W-2 film during the color switch. The coloration time (τ_c) and bleaching time (τ_b) are defined as the time required for a 90% change in the full transmittance modulation at 685 nm, respectively. From the UV-Vis data, the maximum transmittance at the bleached state and the minimum transmittance at the colored state can be obtained, therefore according to the definition, the time required for a 90% change in the full transmittance modulation can be calculated. For W-1, τ_b is found to be 27 s and τ_c is 16 s. For W-2, τ_b is found to be 54 s and τ_c is 30 s. A higher value of τ_c than τ_b for W-1 and W-2 films is might due to the fact of higher diffusion coefficient for lithium ion intercalation than that for deintercalation.[41] Both τ_c and τ_b are higher for W-2 than W-1, indicating that more time is needed for the intercalation/deintercalation of the Li^+ into/out of W-2 because of more tungsten trioxide hydrates formed during the annealing process even though the diffusion coefficient D is higher for W-2 than W-2 which can be calculated from CV.

Coloration efficiency (CE), which is defined as the change in optical density (OD) per unit charge (Q) inserted into (or extracted from) the EC films, is a characteristic parameter for comparing different EC materials. It can be calculated from the following formulas:[66]

$$\eta = \Delta OD(\lambda)/Q_d$$

$$\Delta OD = \log[T_{\text{colored}}/T_{\text{bleached}}]$$

where Q_d is the injected/ejected charges per unit electrode area, and λ is the dominant wavelength for the material. Figure 9 shows the plots of OD change at a wavelength of 685 nm versus the inserted charge density at a potential of −2.0 V. The CE is extracted as the slope of the line fits to the linear region of the curve.[58] The CE is 40.2 cm^2 C^{-1} for W-1 and 48.3 cm^2 C^{-1} and W-2. The higher CE

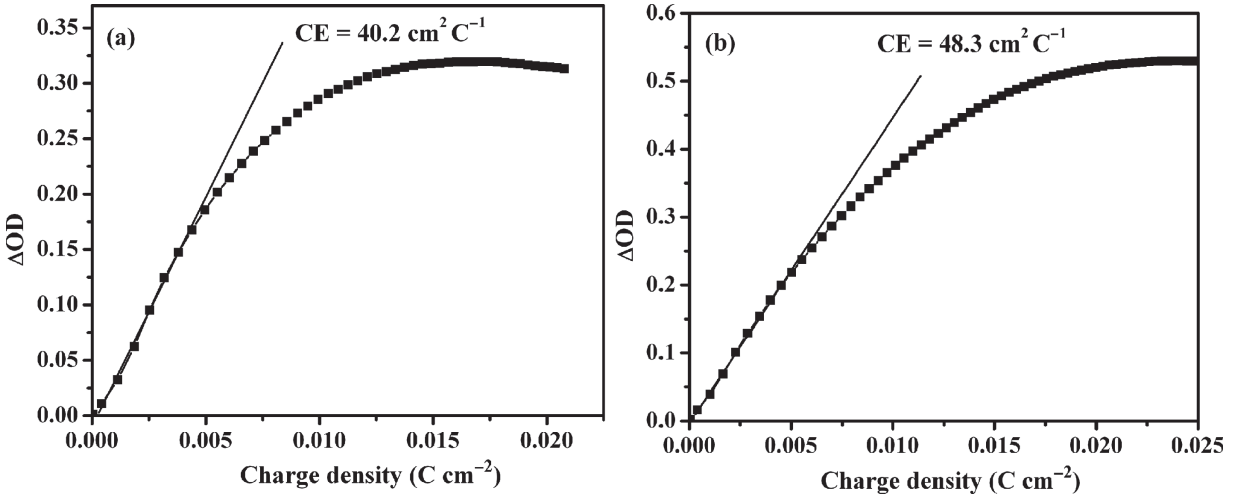

Fig. 9. The plot of *in situ* optical density (OD) change versus charge density of (a) W-1 and (b) W-2 films. The optical density was measured at 685 nm at −2.0 V in 1 M $LiClO_4$ propylene carbonate solution.

for W-2 might be explained by a higher OD change in the coloration/bleaching process which can be confirmed in Figures 6 and 8.

4. CONCLUSION

Electrochromic (EC) tungsten oxide thin films have been successfully prepared by a facile sol–gel process from a tungsten ethoxide/ethanlol/water solution (sol) precursor under different calcination conditions. Amorphous and crystalline structured films were obtained when calcined at 100 °C for 2 h (W-1) or calcined at 100 °C for 2 h followed by 200 °C for another 2 h (W-2), respectively. The results show that W-2 exhibits higher color contrast (30.5% for W-2 and 21.6% for W-1 at 685 nm) and coloration efficiency (40.2 for W-1 and 48.3 cm^2 C^{-1} for W-2), though more time is needed for the coloration and bleaching process. W-2 also displays reproducible color switch even after 1000 cycles of cyclic voltammetry, rendering it promising for applications in solar light control and energy saving in modern buildings.[67]

Acknowledgments: This project is financially supported by the Research Enhancement Grant of Lamar University. J. M. Koziara, P. R. Lockman, D. D. Allen, and R. J. Mumper, J. Nanosci. Nanotechnol. 6, 2712 (2006).

References and Notes

1. D. R. Rosseinsky and R. J. Mortimer, *Adv. Mater.* 13, 783 (**2001**).
2. C. G. Granqvist, *Sol. Energy Mater. Sol. Cells* 60, 201 (**2000**).
3. N. M. Rowley and R. J. Mortimer, *Sci. Prog.* 85, 243 (**2002**).
4. D. T. Gillaspie, R. C. Tenent, and A. C. Dillon, *J. Mater. Chem.* 20, 9585 (**2010**).
5. C. G. Granqvist, *Electrochim. Acta* 44, 3005 (**1999**).
6. S. Y. Choi, M. Mamak, N. Coombs, N. Chopra, and G. A. Ozin, *Nano Lett.* 4, 1231 (**2004**).
7. R. J. Mortimer, A. L. Dyer, and J. R. Reynolds, *Displays* 27, 2 (**2006**).
8. R. J. Mortimer, *Electrochim. Acta* 44, 2971 (**1999**).
9. P. M. S. Monk, R. J. Mortimer, and D. R. Rosseinsky, M. Ltd, Electrochromism: Fundamentals and Applications, VCH Weinheim, Weinheim, Germany (**1995**).
10. C. G. Granqvist, Handbook of Inorganic Electrochromic Materials, Elsevier Science Ltd, Kidlington, England (**1995**).
11. M. İ. Özkut, S. Atak, A. M. Önal, and A. Cihaner, *J. Mater. Chem.* 21, 5268 (**2011**).
12. P. M. Beaujuge and J. R. Reynolds, *Chem. Rev.* 110, 268 (**2010**).
13. J. Zhu, S. Wei, M. J. Alexander, T. D. Dang, T. C. Ho, and Z. Guo, *Adv. Funct. Mater.* 20, 3076 (**2010**).
14. J. Zhu, S. Wei, M. J. Alexander, D. Cocke, T. C. Ho, and Z. Guo, *J. Mater. Chem.* 20, 568 (**2010**).
15. H. Wei, X. Yan, Y. Li, H. Gu, S. Wu, K. Ding, S. Wei, and Z. Guo, *J. Phys. Chem. C* 116, 16286 (**2012**).
16. H. Wei, X. Yan, Y. Li, S. Wu, Y. A. Wang, S. Wei, and Z. Guo, *J. Phys. Chem. C* 116, 4500 (**2012**).
17. B. Yang, Y. Zhang, E. Drabarek, P. R. F. Barnes, and V. Luca, *Chem. Mater.* 19, 5664 (**2007**).
18. M. Shibuya and M. Miyauchi, *Adv. Mater.* 21, 1373 (**2009**).
19. M. Sadakane, K. Sasaki, H. Kunioku, B. Ohtani, R. Abe, and W. Ueda, *J. Mater. Chem.* 20, 1811 (**2010**).
20. J. Solis, S. Saukko, L. Kish, C. Granqvist, and V. Lantto, *Thin Solid Films* 391, 255 (**2001**).
21. Y. S. Kim, S. C. Ha, K. Kim, H. Yang, S. Y. Choi, Y. T. Kim, J. T. Park, C. H. Lee, J. Choi, and J. Paek, *Appl. Phys. Lett.* 86, 213105 (**2005**).
22. C. S. Rout, M. Hegde, and C. Rao, *Sens. Actuators, B* 128, 488 (**2008**).
23. G. Korotcenkov, *Sci. Eng. B* 139, 1 (**2007**).
24. C. Granqvist, G. Niklasson, and A. Azens, *Appl. Phys. A Mater. Sci. Process* 89, 29 (**2007**).
25. G. A. Niklasson and C. G. Granqvist, *J. Mater. Chem.* 17, 127 (**2006**).
26. S. Balaji, Y. Djaoued, A. S. Albert, R. Brüning, N. Beaudoin, and J. Robichaud, *J. Mater. Chem.* 21, 3940 (**2011**).
27. S. H. Lee, R. Deshpande, P. A. Parilla, K. M. Jones, B. To, A. H. Mahan, and A. C. Dillon, *Adv. Mater.* 18, 763 (**2006**).
28. J. Zhang, X. Wang, X. Xia, C. Gu, Z. Zhao, and J. Tu, *Electrochim. Acta* 55, 6953 (**2010**).
29. J. Wang, E. Khoo, P. S. Lee, and J. Ma, *J. Phys. Chem. C* 112, 14306 (**2008**).
30. C. Granqvist, *Sol. Energy Mater. Sol. Cells* 60, 201 (**2000**).
31. R. J. Mortimer, *Annual Review of Materials Research* 41, 241 (**2011**).
32. J. Zhang, J. Tu, X. Xia, X. Wang, and C. Gu, *J. Mater. Chem.* 21, 671 (**2011**).
33. J. Wang, E. Khoo, P. S. Lee, and J. Ma, *J. Phys. Chem. C* 113, 9655 (**2009**).
34. W. Cheng, E. Baudrin, B. Dunn, and J. I. Zink, *J. Mater. Chem.* 11, 92 (**2000**).
35. W. Wang, Y. Pang, and S. N. B. Hodgson, *J. Mater. Chem.* 20, 8591 (**2010**).
36. M. Deepa, T. Saxena, D. Singh, K. Sood, and S. Agnihotry, *Electrochim. Acta* 51, 1974 (**2006**).
37. S. Badilescu and P. Ashrit, *Solid State Ionics* 158, 187 (**2003**).
38. L. LeGore, R. Lad, S. Moulzolf, J. Vetelino, B. Frederick, and E. Kenik, *Thin Solid Films* 406, 79 (**2002**).
39. I. Valyukh, S. Green, H. Arwin, G. Niklasson, E. Wäckelgård, and C. Granqvist, *Sol. Energy Mater. Sol. Cells* 94, 724 (**2010**).
40. L. Krings and W. Talen, *Sol. Energy Mater. Sol. Cells* 54, 27 (**1998**).
41. M. Deepaa, A. K. Srivastavaa, S. Singha, and S. A. Agnihotry, *J. Mater. Res.* 19, 2576 (**2004**).
42. S. M. Kanan and C. P.Tripp, *Curr. Opin. Solid State Mater. Sci.* 11, 19 (**2007**).
43. S. A. Agnihotry, R. Sharma, M. Kar, and T. K. Saxena, *Sol. Energy Mater. Sol. Cells* 90, 15 (**2006**).
44. N. Ozer, *Thin Solid Films* 304, 310 (**1997**).
45. D. J. Taylor, J. P. Cronin, L. F. Allard, and D. P. Birnie, *Chem. Mater.* 8, 1396 (**1996**).
46. D. L. Kepert and J. H. Kyle, *J. Chem. Soc., Dalton Trans.* 1781, 137 (**1978**).
47. A. Takase and K. Miyakawa, *Jpn. J. Appl. Phys.* 30, 1508 (**1991**).
48. G. Ramis, C. Cristiani, A. S. Elmi, and P. Villa, *J. Mol. Catal.* 61, 319 (**1990**).
49. G. Ramis, G. Busca, C. Cristiani, L. Lietti, P. Forzatti, and F. Bregani, *Langmuir* 8, 1744 (**1992**).
50. T. A. Taylor and H. H. Patterson, *Appl. Spectrosc.* 48, 674 (**1994**).
51. A. Tocchetto and A. Glisenti, *Langmuir* 16, 6173 (**2000**).
52. C. Santato, M. Odziemkowski, M. Ulmann, and J. Augustynski, *J. Am. Chem. Soc.* 123, 10639 (**2001**).
53. G. Leftheriotis, S. Papaefthimiou, and P. Yianoulis, *Sol. Energy Mater. Sol Cells* 83, 115 (**2004**).
54. M. Daniel, B. Desbat, J. Lassegues, B. Gerand, and M. Figlarz, *J. Solid State Chem.* 67, 235 (**1987**).
55. B. Orel, N. Groselj, U. O. Krasovec, M. Gabrscek, P. Bukovec, and R. Reisfeld, *Sens. Actuators, B* 50, 234 (**1998**).
56. S. Vaddiraju, H. Chandrasekaran, and M. K. Sunkara, *J. Am. Chem. Soc.* 125, 10792 (**2003**).
57. B. Cao, J. Chen, X. Tang, and W. Zhou, *J. Mater. Chem.* 19, 2323 (**2009**).

ARTICLE

58. J. Zhang, J. Tu, X. Xia, X. Wang, and C. Gu, *J. Mater. Chem.* 21, 5492 **(2011)**.
59. Y. Yao, J. Di, Z. Yong, Z. Zhao, and Q. Li, *Chem. Commun.* 48, 8252 **(2012)**.
60. M. Deepa, R. Sharma, A. Basu, and S. Agnihotry, *Electrochim. Acta* 50, 3545 **(2005)**.
61. M. A. Habib and D. Glueck, *Sol Energy Mater.* 18, 127 **(1989)**.
62. J. Wang, J. M. Bell, and I. L. Skryabin, *Sol. Energy Mater. Sol. Cells.* 59, 167 **(1999)**.
63. J. Wang and J. M. Bell, *Sol. Energy Mater. Sol Cells* 58, 411 **(1999)**.
64. P. R. Somani and S. Radhakrishnan, *Mater. Chem. Phys.* 77, 117 **(2003)**.
65. J. Zhang, J. Tu, D. Zhang, Y. Qiao, X. Xia, X. Wang, and C. Gu, *J. Mater. Chem.* 21, 17316 **(2011)**.
66. P. M. Beaujuge and J. R. Reynolds, *Chem. Rev.* 110, 268 **(2010)**.
67. J. Livage and D. Ganguli, *Sol. Energy Mater. Sol Cells* 68, 365 **(2001)**.